Civil Engineering Dimension
https://ced.petra.ac.id

Experimental Study of Bond Strength of Embedded Steel Reinforcement in Vibration-Based 3D Printed Concrete Mortar

Chandra, J.[1]*, Halim, A.[1], Budiman, F.[1], Pudjisuryadi, P.[1], and Antoni[1]
[1] Civil Engineering Department, Faculty of Civil Engineering and Planning, Petra Christian University
Jl. Siwalankerto 121-131, Surabaya 60236, INDONESIA

DOI: https://doi.org/10.9744/ced.26.2.130-137

Article Info:
Submitted: Mar 05, 2024
Reviewed: Apr 16, 2024
Accepted: Jul 18, 2024

Keywords:
vibration-based 3DCP mortar,
bond strength,
reinforcement diameter,
direction of printing,
building code formulas.

Corresponding Author:
Chandra, J.
Civil Engineering Department,
Faculty of Civil Engineering and Planning, Petra Christian University
Jl. Siwalankerto 121-131, Surabaya 60236, INDONESIA
Email: chandra.jimmy@petra.ac.id

Abstract

Many new construction techniques have been developed in recent years, one of them is Three-Dimensional Concrete Printing (3DCP). It offers many advantages such as reduced human error, minimum manpower usage, and shorter construction period. This technique, however, still needs to be studied further to ensure good quality of constructions. This experimental study aims to investigate the bond strength of embedded steel reinforcement in vibration-based 3DCP mortar. The parameters varied are reinforcement diameter and direction of printing. It is found that average bond stress decreases as reinforcement diameter increases. Furthermore, 3DCP specimens with bars placed parallel to the printing direction have relatively higher bond stresses as compared to the ones with bars placed perpendicularly. As compared to conventional cast specimens, 3DCP specimens have higher bond stresses which might be due to vibration-based 3DCP mortar. Moreover, building code formulas significantly underestimate the bond stresses of vibration-based 3DCP specimens tested in this study.

Introduction

Three-Dimensional Concrete Printing (3DCP) has gained more popularity for research in recent years due to its promising future. Its advantages compared to conventional approach such as, minimized human error, lower labor cost, and shorter construction period are offered by this technology. A lot of research has been conducted to study the mix design, fresh concrete properties, and hardened concrete properties of 3DCP. Each mix design produces different results whether in fresh as well as hardened properties. Up until now, research is still on going to study the relationships between mix design, material processing techniques, and hardened properties of 3DCP [1].

One of the key distinctions of 3DCP lies in its material properties, which are anisotropic, unlike the isotropic properties of conventional concrete. Besides, many factors such as nozzle height, inter-layer printing time gap, nozzle speed, etc. affect the final product of 3DCP which make it difficult to obtain isotropic properties [2]. Past research has been done to study the hardened properties of 3DCP. It was observed that anisotropic properties had significant influence on flexural, shear, and compression capacities of 3DCP [2-3]. It was also observed that subsequent layer moisture level played a major role in the inter-layer strength [3].

Study regarding the behavior of embedded steel reinforcement in 3DCP has been done by Bos et al. [4]. It can be concluded that the chemical reaction between 3DCP mortar and steel reinforcement might deteriorate bond quality. Bond strength tests have shown that in general, conventional cast specimens produce better results as compared to

Note : Discussion is expected before November, 1st 2024, and will be published in the "Civil Engineering Dimension", volume 27, number 1, March 2025.
ISSN : 1410-9530 print / 1979-570X online
Published by : **Petra Christian University**

the 3DCP specimens [4]. This is because of the absence of compaction and the printing procedure which is prone to make cavity in between mortar printed layers.

Studies by Baz et al. [5-6] and Ding at al. [7] regarding bond-slip behavior of 3DCP have discovered that printing direction affects the pull-out strength results. Steel reinforcement which is embedded parallel to the printing direction produced higher pull-out strength results as compared to the one placed in perpendicular direction. Conventional cast specimens have also been shown to produce the highest pull-out strength results as compared to 3DCP specimens [5-7] because the presence of voids between 3DCP layers and steel reinforcement affects the bond strength of 3DCP specimens.

This study aims to explore further the bond strength of embedded steel reinforcement in 3DCP mortar that is produced using 3D printing machine with vibration-based nozzle. The vibration-based nozzle helps produce 3DCP mortar with lesser voids than that of pressure-based nozzle used in previous studies [4-7]. The main variables in this study are the direction of the embedded steel reinforcement to the printing direction and diameter of steel reinforcement. Results from the laboratory pull-out tests will be compared to general concrete building codes such as ACI 318-19 [8] and FIB Model Code 2010 [9].

Laboratory Experiment

Specimen Design

Specimens in this study varied in the direction of embedded steel reinforcement and diameter of the embedded steel. Steel reinforcement was placed in two directions, i.e. parallel and perpendicular to the printing direction of 3DCP mortar as shown in Figure 1. Four types of steel reinforcement were used in this study, i.e. wiremesh M6, wiremesh M8, wiremesh M10, and deformed bar D10. Furthermore, conventional cast specimens were also made as comparison to the 3DCP specimens.

(a) (b)

Figure 1. Steel Reinforcement Placement (a) Parallel to the Printing Direction of 3DCP Mortar, and (b) Perpendicular to the Printing Direction of 3DCP Mortar

Material Properties

Mix design used in this study is shown in Tabel 1. Seven components were used in this mix design which include: Portland cement, water, aggregate, superplasticizer, viscosity modifying agent (VMA), accelerator, and calcium carbonate ($CaCO_3$). The cementitious material used was ordinary Portland cement whereas silica sand with size no more than 0.8 mm was used as the fine aggregate. Superplasticizer (Sika® Viscocrete 1003), VMA (Sika® Stabilizer-4 R), and accelerator (SikaSet® Accelerator) are the admixtures that were used in the mix design. Superplasticizer and VMA were used to improve the flowability and reduce concrete bleeding while accelerator helped the mortar to gain early strength and reduce shrinkage. Calcium carbonate ($CaCO_3$) was used to enhance uniformity of the mixture. Moreover, the properties of steel reinforcement used in this study are shown in Table 2.

Table 1. Mix Design of the 3DCP Mortar

Component	% Cement Weight
Portland cement	100
Sand	150
Water	33
Superplasticizer	0.4
VMA	0.3
Accelerator	4
$CaCO_3$	20

Table 2. Steel Reinforcement Properties

Diameter (mm)	Yield strength (MPa)	Ultimate strength (MPa)	Elongation (%)	Modulus of Elasticity (GPa)
Wiremesh M6	449	499	2.00	180
Wiremesh M8	434	647	9.89	206
Wiremesh M10	401	452	4.12	211
Deformed Bar D10	508	653	17.27	193

Specimen Production

To investigate the bond strength of embedded steel reinforcement, cube specimens with dimensions of 15x15x15 cm were made in this study. Concrete mortar in the conventional cast specimens and the 3DCP specimens utilized the same mix design. In general, steel reinforcement was placed in the concrete cubes at the depth of $5d_b$ (see Figure 2) according to ASTM 234-91A [10] where d_b is the diameter of the embedded steel reinforcement.

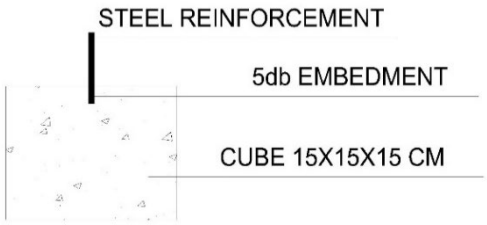

Figure 2. Illustration of the Embedded Steel Reinforcement in the Concrete Cube Specimen

3DCP specimens were printed using gantry-style 3DCP machine at Structural Engineering Laboratory of Petra Christian University, Indonesia (see Figure 3). A vibrated nozzle was used as the extruder of the 3DCP mortar. Printing speed was set at 2 cm/s and the nozzle head tip height was 2 cm above the plywood base. The filament produced in each layer was 5 cm in width and 2 cm in height. In making the 3DCP specimens, a method used by Baz et al. [6] was adopted in this study. Small specimens measuring 5x4x7 cm were produced using the printing machine and then the steel reinforcement was placed manually after one layer was printed (see Figure 4). After the small cubes had hardened, they were placed in the formwork of 15x15x15 cm size and then SikaGrout® 218 was used as filler to fill the space left (see Figure 5). To prevent contact between steel reinforcement and grouting material, two types of protection were introduced, using clear tape and combination of clear tape, PVC pipe, and clay (see Figure 6). Three cube samples were made for each parameter and the specimens coding can be seen in Table 3.

Table 3. Specimens Coding

Code	Remarks
C	conventional cast specimen
Para-I	3D printed specimen with reinforcement placed parallel to printing direction with clear tape protection
Perp-I	3D printed specimen with reinforcement placed perpendicular to printing direction with clear tape protection
Para-P	3D printed specimen with reinforcement placed parallel to printing direction with combination of clear tape, PVC pipe, and clay protection
Perp-P	3D printed specimen with reinforcement placed perpendicular to printing direction with combination of clear tape, PVC pipe, and clay protection

Figure 3. 3D Printing Machine at Structural Engineering Laboratory of Petra Christian University, Indonesia

Figure 4. Printed Small Cubes

Figure 5. Small Cubes Placed in the Formwork (left) and Grouting Material used as Filler (right)

Figure 6. Protection for the Steel Reinforcement using Combination of Clear Tape, PVC Pipe (covered), and Clay

Testing Equipment and Set Up

Pull-out tests were conducted to obtain bond strength of embedded steel reinforcement in the specimens. A test setup similar to the one conducted by Baz et al. [6] was adopted in this study. The specimens were put in a custom steel set up made of two 20 mm thick steel plate measuring 24x24 cm that were connected to each other using four bolts to hold the specimens in place while the reinforcement was being pulled out by a universal testing machine at Concrete Laboratory of Petra Christian University, Indonesia. Full test setup can be seen in Figure 7.

Figure 7. Complete Test Setup

Code Provisions

All pull-out test results would be compared to building code provisions, ACI 318-19 [8] and FIB model code 2010 [9]. Both codes have different approaches in formulating the pull-out stress related to slip. ACI 318-19 [8] only formulates the maximum force capacity in the pulled-out bar while FIB model code 2010 [9] formulates a complete bond-slip relationship of the pulled-out bar. Moreover, FIB model code 2010 [9] also differentiates the formula between good bond condition and other bond conditions.

ACI 318-19 [8] Chapter 17.6.3.2 shows the formula for pull-out failure of anchored bar in concrete. Equation 1 and 2 show the formulas for calculating the pull-out failure. While ACI 318-19 [8] acknowledges splitting failure, the code does not give such formula for calculating this type of failure. Thus, the splitting failure of the specimens would

be compared with the FIB code provision only. Figure 8 shows the bond stress-slip relationship in monotonic loading provided by the FIB model code 2010 [9] while Table 4 shows the formulations.

$$N_p = 8.A_{brg}.fc' \quad (1)$$

$$N_{pn} = \psi_{c,p}.N_p \quad (2)$$

Where:

N_p : Pull-out strength of a single anchor in cracked concrete
A_{brg} : Net area of reinforcement
fc' : Compressive strength of concrete
N_{pn} : Nominal pull-out strength of a single anchor in tension
$\Psi_{c,p}$: Factor used to modify pull-out strength based on presence or absence of cracks in concrete (1.4 for non-cracked concrete, 1.0 for cracked concrete)

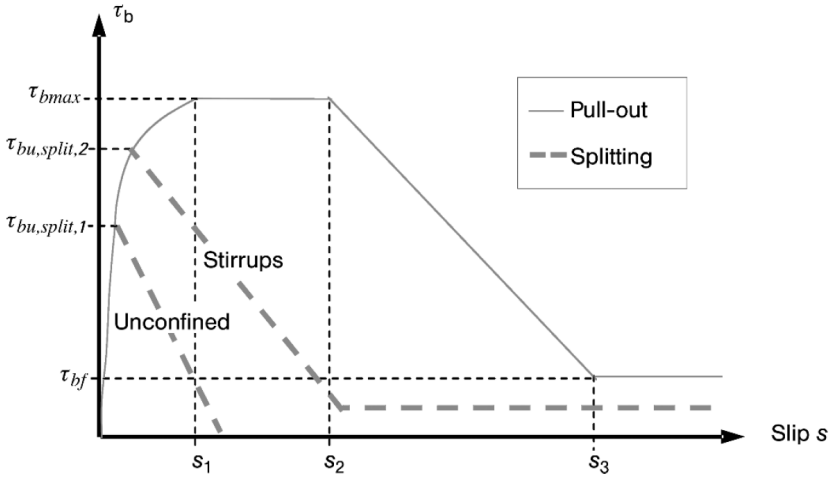

Figure 8. Analytical Bond Stress-slip Relationship in Monotonic Loading [9]

Table 4. Formulations for Different Bond Conditions according to FIB Model Code 2010 [9]

	1	2	3	4	5	6
	Pull-out (PO)		Splitting (SP)			
	$\varepsilon_s < \varepsilon_{s,y}$		$\varepsilon_s < \varepsilon_{s,y}$			
	Good bond cond.	All other bond cond.	Good bond cond.		All other bond cond.	
			Unconfined	Stirrups	Unconfined	Stirrups
τ_{bmax}	$2.5\sqrt{f_{cm}}$	$1.25\sqrt{f_{cm}}$	$2.5\sqrt{f_{cm}}$	$2.5\sqrt{f_{cm}}$	$1.25\sqrt{f_{cm}}$	$1.25\sqrt{f_{cm}}$
$\tau_{bu,split}$	-	-	$7.0 \cdot \left(\frac{f_{cm}}{25}\right)^{0.25}$	$8.0 \cdot \left(\frac{f_{cm}}{25}\right)^{0.25}$	$5.0 \cdot \left(\frac{f_{cm}}{25}\right)^{0.25}$	$5.5 \cdot \left(\frac{f_{cm}}{25}\right)^{0.25}$
s_1	1.0 mm	1.8 mm	$s(\tau_{bu,split})$	$s(\tau_{bu,split})$	$s(\tau_{bu,split})$	$s(\tau_{bu,split})$
s_2	2.0 mm	3.6 mm	s_1	s_1	s_1	s_1
s_3	c_{clear}[1)]	c_{clear}[1)]	$1.2s_1$	$0.5c_{clear}$[1)]	$1.2s_1$	$0.5c_{clear}$[1)]
α	0.4	0.4	0.4	0.4	0.4	0.4
τ_{bf}	$0.40\tau_{max}$	$0.40\tau_{max}$	0	$0.4\ \tau_{bu,split}$	0	$0.4\ \tau_{bu,split}$

Results and Discussion

In general, the experimental results are presented in terms of specimens' pull-out strength, failure mode, and maximum bond stress. There are two failure modes observed during testing, i.e. pull-out (slip) failure and splitting (split) failure (See Figure 9). Tables 5 to 9 show a summary of the maximum pull-out force, failure mode, and maximum pull-out stress for each specimen tested as well as building code predictions.

As can be seen in Tables 5 to 9, in general, the average value of maximum bond stresses decreases as the reinforcement diameter increases, except for conventional cast specimens with wiremesh M6 bar. This is in agreement with current building code [8] which requires bars with larger diameter to have longer development length as compared to smaller bars. Furthermore, similar to the results obtained by Baz et al. [6], in this study, 3DCP specimens with bars parallel to the printing direction have relatively higher bond stresses as compared to the ones with bars perpendicular to the printing direction, except for specimens with wire mesh M8 bar.

(a) (b)

Figure 9. Failure Modes of the Specimens; (a) Pull-out (slip) Failure and (b) Splitting (split) Failure

Table 5. Summary of Test Results for Conventional Cast Specimens

Specimen Name	fc' (MPa)	P (kN)	Failure Mode	τ (MPa)	Average τ (MPa)	ACI [8] τ (MPa)	FIB [9] τ (MPa)
C-M6-1	38.03	4.27	Slip	7.63	8.39	15.21	15.42
C-M6-2		4.53	Slip	8.11			
C-M6-3		5.27	Slip	9.42			
C-M8-1		12.80	Split	13.65	13.56	15.21	15.42
C-M8-2		10.27	Slip	10.95			
C-M8-3		15.07	Slip	16.07			
C-M10-1		12.60	Split	8.36	9.61	-	7.77
C-M10-2		15.33	Split	10.17			
C-M10-3		15.53	Split	10.31			
C-D10-1		21.07	Split	13.78	11.53	-	7.77
C-D10-2		15.60	Split	10.20			
C-D10-3		16.20	Split	10.60			

Table 6. Summary of Test Results for Para-I 3DCP Specimens

Specimen Name	fc' (MPa)	P (kN)	Failure Mode	τ (MPa)	Average τ (MPa)	ACI [8] τ (MPa)	FIB [9] τ (MPa)
Para-I-M6-1	25.32	11.07	Slip	21.62	20.66	10.13	12.58
Para-I-M6-2		10.40	Slip	20.31			
Para-I-M6-3		10.27	Slip	20.05			
Para-I-M8-1		20.20	Slip	21.54	16.16	10.13	12.58
Para-I-M8-2		9.87	Slip	10.52			
Para-I-M8-3		15.40	Slip	16.42			
Para-I-M10-1		21.80	Split	14.47	16.99	-	7.02
Para-I-M10-2		29.40	Split	19.51			
Para-I-M10-3		-	-	-			
Para-I-D10-1		-	-	-	16.35	-	7.02
Para-I-D10-2		22.80	Split	14.91			
Para-I-D10-3		27.20	Split	17.79			

Table 7. Summary of Test Results for Perp-I 3DCP Specimens

Specimen Name	fc' (MPa)	P (kN)	Failure Mode	τ (MPa)	Average τ (MPa)	ACI [8] τ (MPa)	FIB [9] τ (MPa)
Perp-I-M6-1	21.76	9.87	Slip	19.27	20.18	8.70	11.66
Perp-I-M6-2		11.80	Slip	23.05			
Perp-I-M6-3		9.33	Slip	18.23			
Perp-I-M8-1		19.40	Slip	20.69	19.95	8.70	11.66
Perp-I-M8-2		17.27	Slip	18.41			
Perp-I-M8-3		19.47	Slip	20.76			
Perp-I-M10-1		21.00	Split	13.93	13.37	-	6.76
Perp-I-M10-2		23.93	Split	15.88			
Perp-I-M10-3		15.53	Split	10.31			
Perp-I-D10-1		23.33	Split	15.26	12.01	-	6.76
Perp-I-D10-2		15.53	Split	10.16			
Perp-I-D10-3		16.20	Split	10.60			

Table 8. Summary of Test Results for Para-P 3DCP Specimens

Specimen Name	fc' (MPa)	P (kN)	Failure Mode	τ (MPa)	Average τ (MPa)	ACI [8] τ (MPa)	FIB [9] τ (MPa)
Para-P-M6-1	25.32	10.13	Slip	19.79	22.96	10.13	12.58
Para-P-M6-2		9.80	Slip	19.14			
Para-P-M6-3		15.33	Slip	29.95			
Para-P-M8-1		16.93	Slip	18.06	19.12	10.13	12.58
Para-P-M8-2		17.33	Slip	17.23			
Para-P-M8-3		22.20	Slip	22.07			
Para-P-M10-1		26.73	Slip	17.74	15.40	10.13	12.58
Para-P-M10-2		25.73	Split	17.08			
Para-P-M10-3		17.13	Slip	11.37			
Para-P-D10-1		27.47	Split	17.96	18.21	-	7.02
Para-P-D10-2		28.87	Split	18.88			
Para-P-D10-3		27.20	Split	17.79			

Table 9. Summary of Test Results for Perp-P 3DCP Specimens

Specimen Name	fc' (MPa)	P (kN)	Failure Mode	τ (MPa)	Average τ (MPa)	ACI [8] τ (MPa)	FIB [9] τ (MPa)
Perp-P-M6-1	21.76	11.47	Slip	20.51	21.82	8.70	11.66
Perp-P-M6-2		9.80	Slip	17.53			
Perp-P-M6-3		15.33	Slip	27.42			
Perp-P-M8-1		20.20	Slip	21.54	20.88	8.70	11.66
Perp-P-M8-2		17.53	Slip	18.70			
Perp-P-M8-3		21.00	Slip	22.39			
Perp-P-M10-1		13.00	Split	8.63	10.42	-	6.76
Perp-P-M10-2		-	-	-			
Perp-P-M10-3		18.40	Slip	12.21			
Perp-P-D10-1		15.00	Split	9.81	13.91	-	6.76
Perp-P-D10-2		27.53	Split	18.01			
Perp-P-D10-3		-	-	-			

It is worth noting that in this study, 3DCP specimens have higher bond stresses as compared to conventional cast specimens. This is opposite with the results obtained by previous studies [4-7]. This might be due to the difference in the nozzle that was used in the 3D printing machine. Previous studies [4-7] used pressure-based nozzle 3D printing machines without any compaction or vibration and thus the printing method might create voids between 3DCP layers and the steel reinforcement. Therefore, the bond strength of 3DCP specimens is lower as compared to conventional cast specimens that were compacted using external vibrator. In this study, the 3D printing machine employs a vibrator-based nozzle, which effectively compacts the mortar compared to pressure-based nozzles. On the other hand, in this study, the conventional cast specimens were only compacted manually without any external vibrator. Hence, further research is needed to investigate the difference of bond strength between conventional cast specimens and 3DCP specimens if the compaction was done properly using machine or external vibrator.

From the tables, it is evident that for conventional cast specimens, the average maximum bond stresses generally align closely with predictions made by building code formulas [8-9], with the exception of specimens featuring wire mesh M6 bars. On the other hand, for 3DCP specimens, it can be seen that building code formulas [8-9] underestimate the average maximum bond stresses by a significant margin. Therefore, it can be concluded that vibrator-based nozzle used in this study plays an important role in developing bond strength of embedded steel reinforcement. However, further research is needed to investigate this matter with larger reinforcement diameter and various concrete compressive strength.

Conclusions

A total of 60 samples were made for laboratory experiment in this study. From the results of the pull-out tests, several things can be concluded:

1. In general, the average value of maximum bond stresses decreases as the reinforcement diameter increases for both conventional cast and 3DCP specimens. Furthermore, 3DCP specimens with bars placed parallel to the printing direction have relatively higher maximum bond stresses as compared to the ones with bars placed perpendicular to the printing direction. This finding is in agreement with previous study by Baz et al. [6].

2. In contrast with previous studies by Bos et al. [4], Baz et al. [5-6], and Ding et al. [7], in this study, 3DCP specimens have higher bond stresses as compared to conventional cast specimens. This might be due to the vibrator-based nozzle used in the 3D printing machine in this study that produced mortar with lesser voids than that of pressure-based nozzle used in previous studies. Nevertheless, further research is needed to confirm this hypothesis.
3. ACI 318-19 [8] and FIB model code 2010 [9] significantly underestimate the bond stresses of 3DCP specimens that were printed using vibrator-based nozzle in this study. However, further research with larger reinforcement diameter and various concrete strength is needed to confirm this conclusion.

Acknowledgments

The authors are grateful for the funding provided by Petra Christian University.

References

1. Bos, F., Wolfs, R., Ahmed, Z., and Salet, T., Additive Manufacturing of Concrete in Construction: Potentials and Challenges of 3D Concrete Printing, *Virtual and Physical Prototyping*, *11*(3), 2016, pp. 1-17.
2. Paul, S.C., Tay, Y.W.D., Panda, B., and Tan, M.J., Fresh and Hardened Properties of 3D Printable Cementitious Materials for Building and Construction, *Archives of Civil and Mechanical Engineering*, *18*, 2018, pp. 311-319.
3. Sanjayan, J.G., Nematollahi, B., Xia, M., and Marchment, T., Effect of Surface Moisture on Inter-layer Strength of 3D Printed Concrete, *Construction and Building Materials*, *172*, 2018, pp. 468-475.
4. Bos, F., Dezaire, S., Ahmed, Z., Hoekstra, A., and Salet T., Bond of Reinforcement Cable in 3D Printed Concrete, *RILEM Book Series*, *28*, 2020, pp. 584-600.
5. Baz, B., Aouad, G., and Remond, S., Effect of the Printing Method and Mortar's Workability on Pull Out Strength of 3D Printed Concrete, *Construction and Building Materials*, *230*, 2020, pp. 1-8.
6. Baz, B., Aouad, G., Leblond, P., Al-Mansouri, O., D'hondt, M., and Remond, S., Mechanical Assessment of Concrete-Steel Bonding in 3D Printed Elements, *Construction and Building Materials*, *256*, 2020, pp. 1-11.
7. Ding, T., Qin, F., Xiao, J., Chen, X., and Zuo, Z., Experimental Study on the Bond Behaviour between Steel Bars and 3D Printed Concrete, *Journal of Building Engineering*, *49*, 2022, pp. 1-15.
8. ACI 318-19, *Building Code Requirements for Structural Concrete*, American Concrete Institute, 2019.
9. FIB, *fib Model Code for Concrete Structures 2010*, International Federation for Structural Concrete, 2010.
10. ASTM International, *Standard Test Method for Comparing Concretes on the Basis of the Bond Developed with Reinforcing Steel – ASTM C234-91a*, American Society for Testing and Materials, 1991.